ADVANCED ELECTRONIC MATERIALS
www.advelectronicmat.de

Manipulating the Molecular Backbone to Achieve Highly Emissive Sky-Blue AIEgens and Their Applications in Nondoped Organic Light-Emitting Diodes

Dongfeng Dang, Zhiheng Wang, Kunkun Liu, Yong Liu, Herman H. Y. Sung, Ian D. Williams, Ryan T. K. Kwok, Jacky W. Y. Lam, Shi-Jian Su, and Ben Zhong Tang**

To enhance the luminescent performance of aggregation-induced emission luminogens (AIEgens) in organic light-emitting diodes (OLEDs) but also retain their blue emission color, 2-CzTPE and 2,7-CzTPE with promising AIE features are synthesized to balance the trade-off between twisted molecular conformation and enlarged molecular conjugation. As observed, although 2-CzTPE, which contains twisted molecular backbone, could suppress the emission-quenching π–π stacking, an inferior luminescent performance with photoluminescence quantum yields (PLQYs) of 23.12% occurs in aggregated solid state for its limited molecular conjugation, then leading to an inferior electroluminescence (EL) performance with external quantum efficiency (EQE) of 1.9%. However, after molecular engineering of backbone to enlarge its conjugation in 2,7-CzTPE, significantly enhanced PLQY value of 60.63% is achieved in solid state. Interestingly, the emission of 2,7-CzTPE remains in the blue region, which is even identical to that of 2-CzTPE in aggregates. Finally, much better EL performance in nondoped OLEDs with current efficiency of 7.38 cd A^{-1}, power efficiency of 6.81 lm W^{-1}, and also EQE of 3.0% is achieved for 2,7-CzTPE-based devices. These findings demonstrate that manipulating molecular backbone to achieve the balanced molecular conjugation and twisted conformation is an efficient way to obtain highly emissive blue AIEgens in both aggregated state and OLEDs devices.

1. Introduction

Over the past few decades, organic light-emitting diodes (OLEDs) have attracted tremendous attentions for their promising applications in solid-state lighting.[1] To achieve this real-world application, organic luminescent materials (OLMs) have been demonstrated to play important roles as emitters in OLEDs.[2] Owing to these recent efforts in novel OLMs,[3] a number of high-performance OLEDs have been developed, especially for those in red and green colors.[4,5] However, to obtain full-color displays in OLEDs, blue emitters with good stability and also remarkable electroluminescence (EL) performance are also necessary.[6] Unfortunately, unlike the red and green emitters, highly emissive blue OLMs in devices are rare due to their wide bandgap, but recently it has been demonstrated that OLMs with impressive and robust solid-state photoluminescence (PL) efficiency is beneficial to enhance their EL performance in OLEDs significantly.[7] Therefore, developing highly emissive blue OLMs in aggregated solid state becomes one of the key procedures to achieve the corresponding efficient OLEDs.

For most conventional OLMs, impressive emissive features can be obtained in their dilute solutions, while weak or completely quenched emission was observed in the solid state for

Dr. D. Dang, Dr. Y. Liu, Dr. H. H. Y. Sung, Prof. I. D. Williams, Prof. R. T. K. Kwok, Prof. J. W. Y. Lam, Prof. B. Z. Tang
Department of Chemistry
Hong Kong Branch of Chinese National Engineering Research Center for Tissue Restoration and Reconstruction
Division of Life Science
State Key Laboratory of Molecular Neuroscience
Institute for Advanced Study
Institute of Molecular Functional Materials
Division of Biomedical Engineering
The Hong Kong University of Science and Technology
Clear Water Bay, Kowloon, Hong Kong 999077, China
E-mail: tangbenz@ust.hk

The ORCID identification number(s) for the author(s) of this article can be found under https://doi.org/10.1002/aelm.201800354.

DOI: 10.1002/aelm.201800354

Dr. D. Dang
School of Science
MOE Key Laboratory for Nonequilibrium Synthesis and Modulation of Condensed Matter
Xi'an Jiaotong University
Xi'an 710049, China

Z. Wang, K. Liu, Prof. S.-J. Su, Prof. B. Z. Tang
State Key Laboratory of Luminescent Materials and Devices
South China University of Technology
Guangzhou 510640, China
E-mail: mssjsu@scut.edu.cn

Prof. B. Z. Tang
Guangdong Provincial Key Laboratory of Brain Science Disease and Drug Development
HKUST-Shenzhen Research Institute
No. 9 Yuexing 1st RD, South Area, Hi-tech Park, Nanshan
Shenzhen 518057, China

the detrimental aggregation-caused quenching (ACQ). Interestingly, several efficient methods to avoid the aggregation of OLMs have been established and then prevent the ACQ phenomenon. For instance, Yin and co-workers incorporated dendrimer as an outshell to suppress the aggregation of organic chromophore and then provide the strategy to overcome ACQ problems.[8] However, it should be mentioned that although impressive performance can be obtained in some cases, the complicated procedures and uncontrollable phase separation usually limit their further applications.[9] In 2001, Tang and his co-workers observed a unique photophysical phenomenon of "aggregation-induced emission (AIE),"[10] in which OLMs in solution state exhibited weak or no emission, but those in aggregated states had remarkable luminescent characteristics.[11] Since then, AIE has been considered as one of the most powerful strategy for overcoming ACQ effect and the corresponding AIE luminogens (AIEgens) with high solid-state PL efficiency are frequently used as emitters in OLEDs.[12] For instance, an efficient AIE-active blue emitter based on tetraphenylsilane (CzPySiTPE) was reported by Lu et al. and then successfully used in the high-performance deep-blue OLEDs with an external quantum efficiency (EQE) of 1.12%.[13] Furthermore, for the conventional OLEDs, guest–host systems are usually applied to enhance their device performance. Although it can work well in some cases, additional complexity and also cost limit their mass production in OLEDs seriously. Moreover, the unstable phase separations for these reported guest–host systems upon heating could also result the performance degradation. Therefore, high-performance nondoped OLED devices are urgently needed. Encouragingly, using highly emissive AIEgens as emitters in OLEDs provided the pragmatic platform to solve these problems and then afforded the efficient nondoped OLEDs.[14]

To afford AIEgens with efficient blue emission in OLEDs, carbazole building block (Cz) has received great attentions for their merits of high carrier mobility, good emission efficiency, and also impressive chemical stability.[15] In addition, tetraphenylethene (TPE) and its derivatives have also been used to construct highly emissive AIEgens in OLEDs.[16] Based on their impressive merits, deep or sky-blue AIEgens based on carbazole and tetraphenylethene units, such as 2TPE (2,7) and DPVTCz (**Scheme 1**), were reported and employed to afford efficient OLEDs devices.[17] Nonetheless, the luminescent performance for these AIEgens in OLEDs should be further enhanced so that their applications in solid-state displays can be fulfilled. Interestingly, to obtain high-performance AIEgens-based OLEDs, two opposing factors are required in molecular design: twisted molecular conformation is required to suppress emission-quenched π–π stacking; and enlarged molecular conjugation is sufficient to guarantee intermolecular interactions and also charge carrier transport. In some cases, blue AIEgens with largely twisted molecular backbone can only exhibit inferior device performance for their limited conjugation. On the other hand, although some AIEgens with enlarged molecular conjugations exhibited enhanced emission efficiency that leads to improved performance in devices, the emitted blue color can also be easily shifted. Therefore, to enhance the luminescent performance of AIEgens in OLEDs but also retain their blue emission color, a balance between the twisted molecular conformation and enlarged molecular conjugation should be reached. Recently, Li and co-workers developed several AIEgens with blue emission in OLEDs, in which the molecular conjugation was controlled through twisted linkages in their chemical backbones.[18] Moreover, methylTPA-3pTPE, one of the blue AIEgens with emissive features in solid states, was also shown to exhibit impressive EL performance with a remarkable current efficiency (CE) of 8.03 cd A^{-1} and EQE value of up to 3.99%.[19] Inspired by this work, 2-CzTPE and 2,7-CzTPE with promising AIE features were synthesized here to balance the trade-off between twisted molecular conformation and enlarged molecular conjugation, and their relationships between molecular structures and luminescent performance were also investigated in details. The observations showed that although 2-CzTPE exhibited a twisted molecular backbone to suppress the emission-quenching π–π stacking in aggregated state, its limited molecular conjugation resulted in an inferior luminescent performance with quantum yield of 23.12%. However, after manipulating the molecular backbone to enlarge the molecular conjugation in 2,7-CzTPE, significantly enhanced photoluminescence quantum yields (PLQYs) value of up to

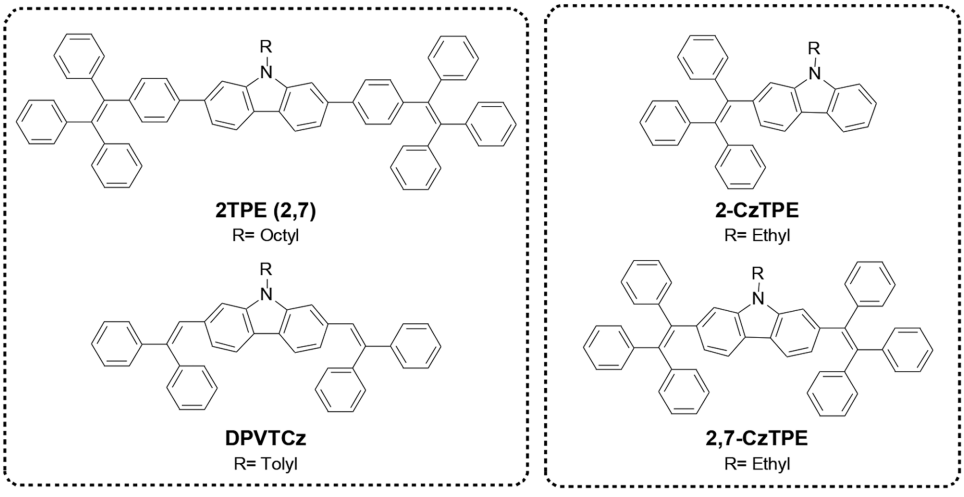

Scheme 1. The chemical structures of 2TPE (2,7), DPVTCz, 2-CzTPE, and 2,7-CzTPE.

60.63% was achieved in solid state. Interestingly, although these molecular skeletons are different, the emission spectra for 2-CzTPE and 2,7-CzTPE were almost identical. Furthermore, suitable highest occupied molecular orbital (HOMO) and lowest unoccupied molecular orbital (LUMO) energy levels for 2-CzTPE and 2,7-CzTPE indicated both molecules exhibited good hole/electron injection ability in OLEDs. Therefore, the nondoped OLED devices with a structure of ITO/HATCN/NPB/TCTA/EML (2-CzTPE or 2,7-CzTPE)/TPBI/LiF/Al were further fabricated. Similar to the reported OLEDs based on 2TPE (2,7) and DPVTCz,[17] 2-CzTPE-based OLEDs exhibited an inferior EL performance with a CE value of 4.08 cd A^{-1}, a power efficiency (PE) value of 3.36 lm W^{-1}, and an EQE value of 1.9%. However, much better EL performance was achieved for 2,7-CzTPE in nondoped OLEDs with the maximum CE, PE, and EQE values of 7.38 cd A^{-1}, 6.81 lm W^{-1}, and 3.0%, respectively. The findings indicate that the established sky-blue AIEgen of 2,7-CzTPE with balanced trade-off between molecular conjugation and twisted conformation is highly emissive in aggregated solid states and can effectively be used as a blue emitter in the efficient nondoped OLEDs.

2. Results and Discussion

2.1. Synthesis and Thermal Properties

Chemical structures of target molecules (2-CzTPE and 2,7-CzTPE) are displayed in Scheme 1, and their synthetic routes are outlined in Scheme S1 (Supporting Information). Both 2-CzTPE and 2,7-CzTPE were obtained with high yields through Suzuki coupling reaction using commercially available bromotriphenylethylene and easily prepared 9-ethyl-2-(4,4,5,5-tetramethyl-[1,3,2]dioxaborolan-2-yl)-9H-carbazole or 9-ethyl-2,7-bis-(4,4,5,5-tetra-methyl-[1,3,2]dioxaborolan-2-yl)-9H-carbazole as the starting materials.[20] Then, after purification using silica gel column chromatography, the chemical structures of 2-CzTPE and 2,7-CzTPE were characterized and confirmed through ^{1}H NMR, ^{13}C NMR, and matrix-assisted laser desorption/ionization–time-of-flight mass spectrometry (MALDI-TOF MS) spectra (Supporting Information).

Because thermal stability of organic emitters plays an important role in long-lived OLEDs, thermal properties of 2-CzTPE and 2,7-CzTPE were investigated here using thermogravimetric analysis (TGA) and differential scanning calorimetry (DSC). As summarized in **Table 1**, the decomposition temperatures (T_d), corresponding to a 5% weight loss, were observed as high as 282.7 and 366.6 °C for 2-CzTPE and 2,7-CzTPE (Figure S1, Supporting Information), indicating that 2,7-CzTPE with enlarged molecular skeleton has better thermal stability. Additionally, the DSC thermograms showed distinct glass transition temperatures (T_g) for both 2-CzTPE and 2,7-CzTPE at 77.2 and 138.4 °C, followed by recrystallization at 151.1 and 185.2 °C, and melting points (T_m) at 199.1 and 319.7 °C, respectively (Figure S2, Supporting Information). The much better thermal properties here for 2,7-CzTPE in contrast to that in 2-CzTPE demonstrated its promising potentials in the application of stable OLEDs.[21]

2.2. Optical Properties

The ultraviolet–visible (UV–vis) absorption spectra of 2-CzTPE and 2,7-CzTPE in tetrahydrofuran (THF, [c] = 5×10^{-5} M) and thin films were then investigated (Figure S3, Supporting Information). Similar absorption spectra in a wavelength range from 200 to 425 nm were obtained for both molecules. Additionally, only slight redshifts were observed for 2-CzTPE and 2,7-CzTPE in their absorption profiles from solution to thin films due to their twisted molecular structures, indicating the much weak intermolecular π–π stacking for both 2-CzTPE and 2,7-CzTPE in solid states. This observed weak π–π stacking is also demonstrated to be beneficial to achieving good fluorescent performance in aggregated states, such as AIE characteristics.[22] Therefore, PL spectra in THF solution for 2-CzTPE and 2,7-CzTPE were first measured. As anticipated, no or weak emission features for 2-CzTPE and 2,7-CzTPE in THF solution (solution state) were observed.[23] After that, PL spectra for both molecules in THF/water mixture containing different fractions of water (f_w) were then collected. As illustrated in **Figure 1**a,b, similar to that observed in dilute solution, weak emission intensities were observed until f_w reached 70%. Then the emission was finally significantly enhanced when f_w reached 90%, whereby aggregates were largely formed. It should be noted that although the enlarged molecular skeleton was employed in 2,7-CzTPE (in contrast to 2-CzTPE), the proposed molecular conjugation was controlled well through the twisted molecular backbone, which also prevented the emission quenched π–π stacking. Therefore, similar sky-blue emission spectra and chromaticity coordinates in sky-blue region were observed for both 2-CzTPE and 2,7-CzTPE in their aggregated states with f_w of 90% (Figure 1c and Table 1). To further investigate their AIE properties in more details, relative PL intensities (I/I_0) for 2-CzTPE and 2,7-CzTPE were also plotted and compared here (Figure 1d). The plots showed that large I/I_0 values of up to 386 and 492 were observed for 2-CzTPE and 2,7-CzTPE, respectively. On the other hand, to investigate their AIE features much better, the solvent system of THF and methanol was also employed here. It is observed in this case aggregation can be hardly obtained when methanol was added to their

Table 1. Thermal properties and photophysical properties for 2-CzTPE and 2,7-CzTPE.

Compounds	Thermal properties	PL				CV	
	T_d [°C]	λ_{em}[a)] [nm]	CIE[a)] coordinates	QY[b)] [%]	τ[b)] [ns]	HOMO[c)] [eV]	LUMO[d)] [eV]
2-CzTPE	282.7	489.6	0.18,0.34	23.12	1.6	−5.41	−2.21
2,7-CzTPE	366.6	489.8	0.17,0.34	60.63	2.9	−5.42	−2.52

[a)]Measured in THF/water mixture (f_w = 90%); [b)]Measured in solids; [c)]Measured in CH_3CN solution by CV method; [d)]Calculated by HOMO energy levels and their corresponding optical gaps.

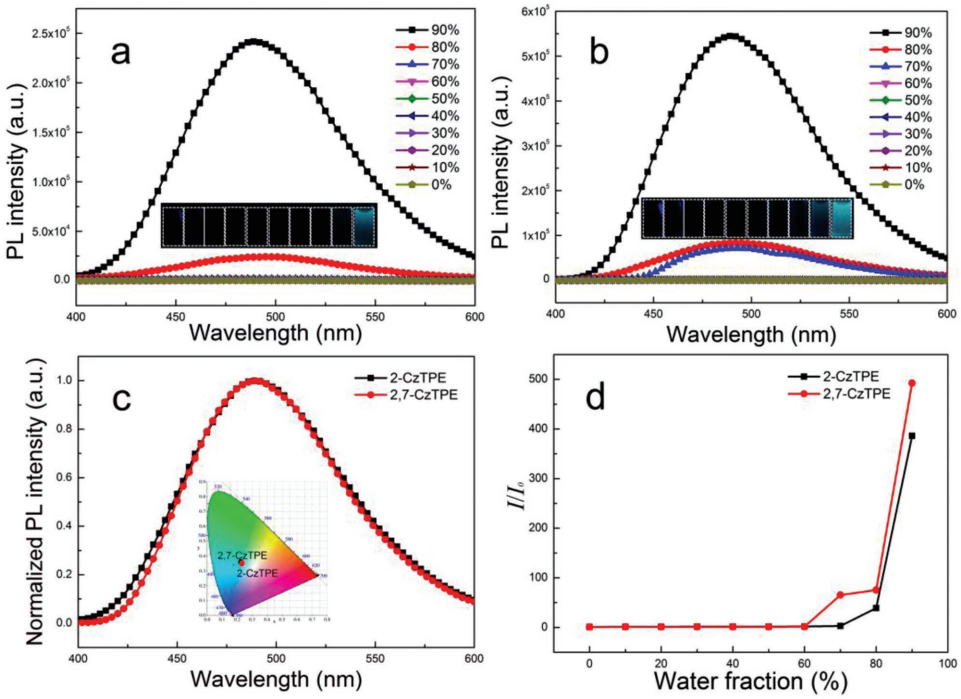

Figure 1. a,b) PL spectra of 2-CzTPE and 2,7-CzTPE in THF with different fractions of water (the inset shows the corresponding luminescent photos under UV light); c) normalized PL spectra of 2-CzTPE and 2,7-CzTPE in aggregated states with f_w of 90% (the inset shows the corresponding chromaticity coordinates); d) variation of PL intensities (I/I_0) for 2-CzTPE and 2,7-CzTPE in THF with different f_w.

corresponding THF solution gradually, thus resulting in no or weak emission features even when the methanol fraction (f_m) is 90% (Figures S4 and S5, Supporting Information). However, several days later, it is interesting that some precipitates can be obviously observed in this new system (f_m = 90%), which were then investigated under a fluorescence microscope and a scanning electronic microscope (SEM). Although amorphous morphologies were captured, emissive characteristics can be observed for both compounds (Figure S6, Supporting Information). The result here further indicates that these developed molecules here are truly the promising AIEgens.

Moreover, in the THF/water systems, when f_w reached 70%, a large quantity of precipitations was observed in both 2-CzTPE and 2,7-CzTPE. The precipitates were then also investigated under a fluorescence microscope and SEM. As displayed in **Figure 2**, nanofibers were observed for both molecules. Then, the observations were further confirmed by using X-ray diffraction (Figure S7, Supporting Information), from which sharp peaks were obtained, especially for 2,7-CzTPE, indicating that well-ordered molecular packing in the aggregated states occurred here for 2,7-CzTPE. The results demonstrate that despite the introduction of twisted molecular backbones into 2,7-CzTPE, some intermolecular interactions caused by its enlarged molecular conjugation, such as C—H$\cdots\pi$ interactions, remain strong in their aggregated states and, in turn, lead to uniform molecular packing that results in crystalline nanoprecipitations. It is also worth noting that these ordered fibers can be easily precipitated for 2,7-CzTPE, whereas, much longer time takes for 2-CzTPE, which further demonstrated the efficient packing and C—H$\cdots\pi$ interactions in 2,7-CzTPE. Interestingly, the emission color for these fibers here is a little different from that in Figure 1c, which is probably caused by their altered intermolecular interactions and also molecular packing. Although slight redshift was observed for these fiber-like 2,7-CzTPE, the observed uniform molecular packing and intermolecular interactions were demonstrated to not only benefit their emission efficiency in solid state, but also favor its charge transfer performance in OLED devices.[24] Therefore, according to the results here, the developed sky-blue 2,7-CzTPE can be a good candidate for the high-performance and ultrabright OLEDs. On the other hand, the fluorescence and SEM images for the other aggregated states with f_w of 80 and 90% were also captured here (Figures S8 and S9, Supporting Information). However, only the amorphous morphologies were observed for both 2-CzTPE and 2,7-CzTPE owing to their hydrophobic properties and the large water contents in both cases.

The absolute emission quantum yields for these developed sky-blue AIEgens were then measured here. Similar to their emission intensities in dilute solution, inferior emission efficiencies with negligible PLQY values of 0.22 and 0.36% were observed for 2-CzTPE and 2,7-CzTPE in dilute solution, respectively (**Figure 3**a). Such emission efficiencies were then significantly increased in aggregated states. Among them, moderate PLQY value of 23.12% was obtained in 2-CzTPE. By contrast, larger PLQY value of up to 60.63% was achieved for 2,7-CzTPE. It is possible that the molecular conjugation and twisted molecular conformation is balanced here in 2,7-CzTPE to afford efficient intermolecular interactions and also avoid emission-quenched π–π stacking, thus exhibiting such high emission efficiency. To further understand the emission efficiency of 2-CzTPE and 2,7-CzTPE, time-resolved PL spectra

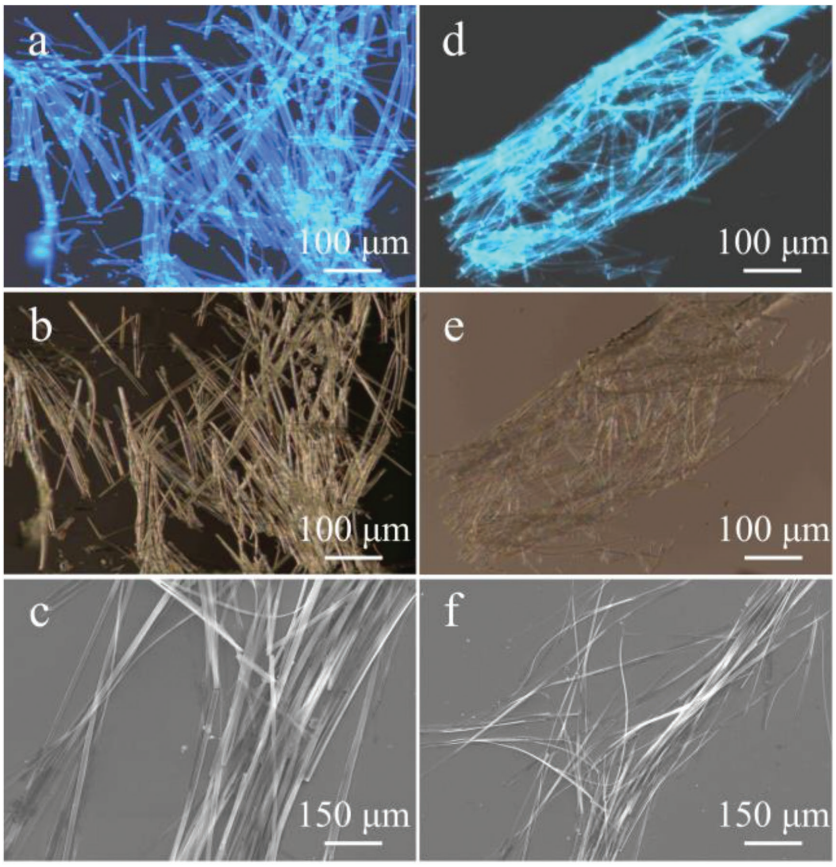

Figure 2. Fluorescence images of aggregates for 2-CzTPE (left) and 2,7-CzTPE (right) under a,d) dark field and b,e) bright field with a f_w of 70%; c,f) SEM images of aggregates for 2-CzTPE and 2,7-CzTPE with a f_w of 70%.

were measured and the corresponding decay curves are illustrated in Figure 3b. Compared with that of 2-CzTPE (1.6 ns), the lifetime (τ) of 2,7-CzTPE was much longer (2.9 ns). Based on these data, the radiative decay rates (k_r) and the nonradiative decay rates (k_{nr}) were calculated according to the equations: $k_r = QY/\tau$ and $k_{nr} = 1/\tau - k_r$.[25] Interestingly, compared with 2-CzTPE ($k_r = 1.4 \times 10^8$ s^{-1}; $k_{nr} = 4.8 \times 10^8$ s^{-1}), increased k_r value of 2.1×10^8 s^{-1} and also decreased k_{nr} value of 1.3×10^8 s^{-1} were simultaneously achieved for 2,7-CzTPE. These observations further explain the much higher emission efficiency of 2,7-CzTPE in solid states.

2.3. Molecular Packing and Theoretical Calculations

To further understand their different emissive natures, we tried to prepare the single crystals for both 2-CzTPE and 2,7-CzTPE. Although several solvent systems were applied for 2-CzTPE, its single crystal cannot be prepared here. However, single crystal of 2,7-CzTPE was successfully obtained in THF/*n*-hexane mixture. As illustrated in **Figure 4**a,b, 2,7-CzTPE exhibited twisted conformation with a large dihedral angle of 55.06°. This largely twisted molecular backbone is beneficial to weaken the molecular conjugation to some extent. Therefore, it can be understandable similar emission spectra was observed for 2,7-CzTPE when compared with 2-CzTPE. Additionally, such twisted conformation could also result in the large packing distances between neighboring planes (5.431 and 9.503 Å, respectively). Therefore, the emission-quenching caused by π–π stacking in aggregated states can also be efficiently prevented (Figure 4c). Furthermore, the other intermolecular interactions in the crystal structure of 2,7-CzTPE, such as C—H$\cdots\pi$ interactions, were also found to restrain the molecular motions effectively (Figure 4d). These results further demonstrate that the balanced trade-off between molecular conjugation and twisted conformation was reached in the developed AIEgen of 2,7-CzTPE.

To make a better comparison, the ground-state geometries of 2-CzTPE and 2,7-CzTPE were then calculated and optimized using DFT at B3LYP/6-31G** level. As displayed in **Figure 5**, both 2-CzTPE and 2,7-CzTPE contained twisted molecular conformations with large dihedral angles of 49.20° and 49.54°, respectively. To further gain insights into their electronic

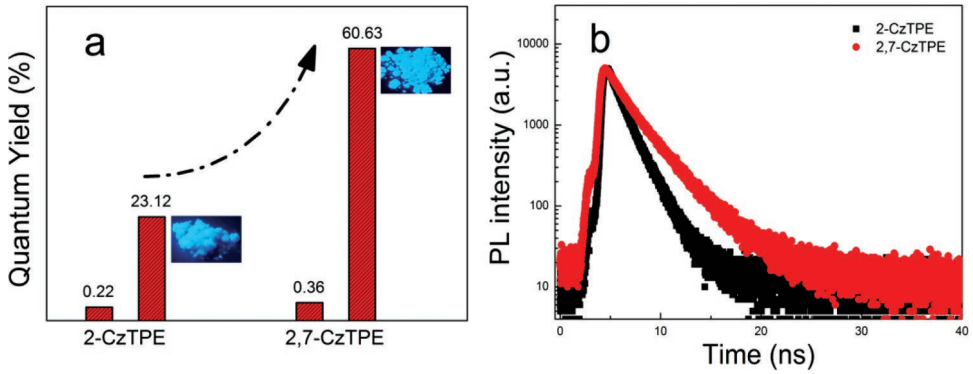

Figure 3. a) Quantum yields of 2-CzTPE and 2,7-CzTPE in solution and solid state (the inset shows their corresponding emission powders); b) transient decay spectra of 2-CzTPE and 2,7-CzTPE in aggregated solid state.

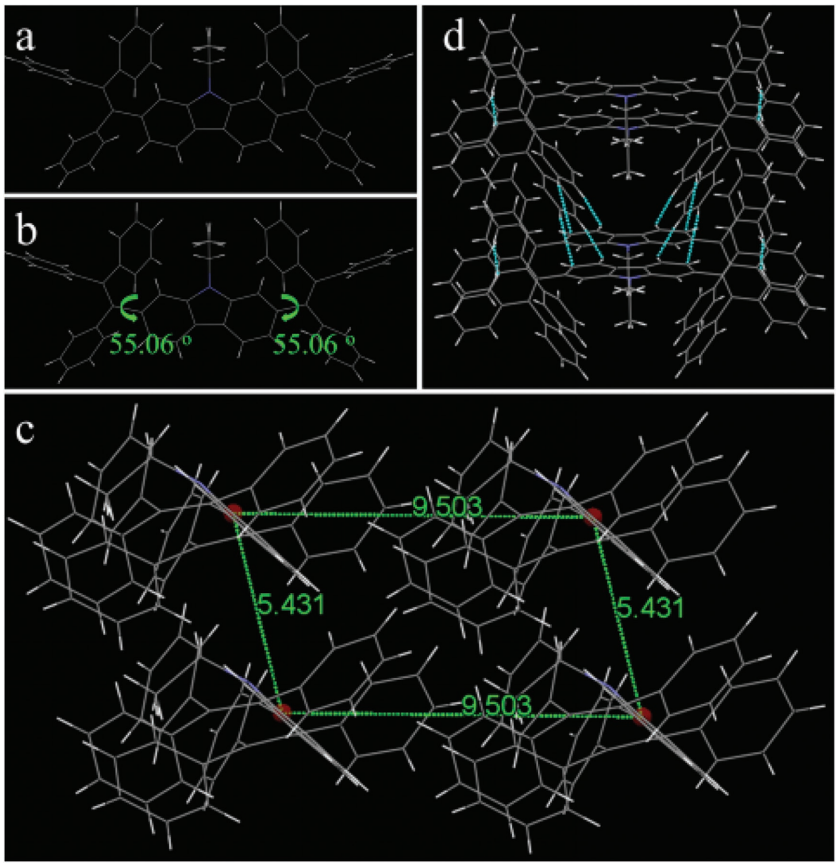

Figure 4. a) Crystal structure and b) twist angle for 2,7-CzTPE; c) intermolecular stacking distance and d) intermolecular interactions (green dashed lines) for 2,7-CzTPE.

structures, distributions of the HOMO and the LUMO for 2-CzTPE and 2,7-CzTPE were also studied. Both HOMOs and LUMOs were located in the molecular backbones, whereby local electronic clouds are distributed. The calculated HOMO and LUMO energy levels for 2-CzTPE and 2,7-CzTPE were –5.12/–1.28 and –4.97/–1.38 eV, respectively, suggesting that these sky-blue AIEgens can be used as organic emitters in OLEDs devices. It should also be mentioned that although different energy gaps were observed in 2-CzTPE and 2,7-CzTPE here, similar emission spectra in aggregated states were still achieved (THF with f_w of 90%), indicating that not only their own electronic structures, but also the intermolecular interactions should be considered here. For 2,7-CzTPE, two triphenylethylene units were linked to the carbazole building blocks to afford the twisted conformations. Therefore, the intermolecular interactions to redshift the emission spectra or weaken their emission features, such as π–π stacking, can be fully avoided, finally leading to the similar blue emission spectra but with enhanced emission efficiency in 2,7-CzTPE.

2.4. Electrochemical Properties

The electrochemical properties of 2-CzTPE and 2,7-CzTPE were then investigated by using cyclic voltammetry (CV) method, and the corresponding data are summarized in Table 1. The onset oxidation potentials ($E_{ox.vs\ Fc/Fc^+}$) for 2-CzTPE and 2,7-CzTPE, which were calibrated against ferrocene/ferrocenium (Fc/Fc^+) redox couple, were 0.61 and 0.62 V, respectively (**Figure 6**a). The reduction potentials for 2-CzTPE and 2,7-CzTPE, calculated by these oxidation potentials and their corresponding optical gaps, were –2.59 and 2.28 V, respectively. Then the energy levels (E_{HOMO}/E_{LUMO}) for the developed AIEgens were calculated according to the following equations[26]

$$E_{HOMO}(eV) = -(E_{ox.vsFc/Fc^+} + 4.8)$$

$$E_{LUMO}(eV) = -(E_{re.vsFc/Fc^+} + 4.8)$$

Finally, the HOMO and LUMO energy levels of –5.41/–2.21 and –5.42/–2.52 eV were determined for 2-CzTPE and 2,7-CzTPE, respectively. As displayed, similar HOMO energy levels were observed for both

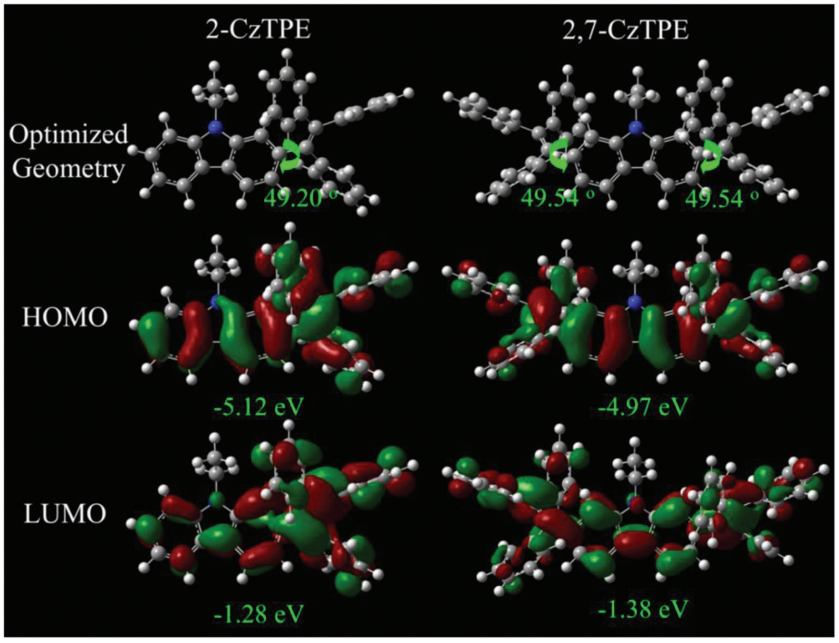

Figure 5. The optimized geometry, HOMO and LUMO energy level diagrams for 2-CzTPE and 2,7-CzTPE using DFT.

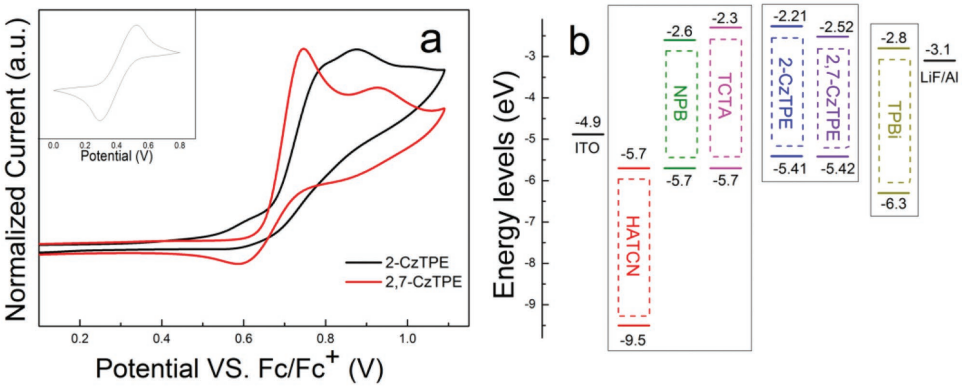

Figure 6. a) CV curves of 2-CzTPE and 2,7-CzTPE on Pt electrode in 0.1 M Bu_4NPF_6, CH_3CN solution (the inset shows CV curves of Fc/Fc^+ couple); b) schematic energy diagram of HATCN, NPB, TCTA, 2-CzTPE, 2,7-CzTPE, and TPBi.

2-CzTPE and 2,7-CzTPE, which is also very close to that of 4,4′-bis[(1-naphthyl)(phenyl) amino]-biphenyl (NPB, –5.70 eV, Figure 6b). Therefore, small potential barrier here for both compounds can be observed, then leading to good hole-injection ability. In contrast, after one more TPE unit was introduced into 2,7-CzTPE, the LUMO energy levels of 2,7-CzTPE were largely decreased (–2.52 eV), which is even comparable to those widely used electron-transporting materials of 1,3,5-tris(1-phenyl-1*H*benzimidazol-2-yl)benzene (TPBi, –2.8 eV, Figure 6b), thus small potential barrier and also excellent electron-injection ability can be expected in the corresponding OLED devices.[27]

2.5. Electroluminescence in Nondoped OLEDs

Owing to their good thermal stability, suitable energy levels, and remarkable light emissions, the nondoped OLED devices with a structure of ITO/HATCN (5 nm)/NPB (40 nm)/TCAT (5 nm)/EML (20 nm)/TPBI (40 nm)/LiF/Al using 2-CzTPE and 2,7-CzTPE as emitters were fabricated here to explore their potential applications in highly efficient OLEDs (**Figure 7**a). In the devices, dipyrazino[2,3-f:2′,3′-*h*]quinoxaline-2,3,6,7,10,11-hexacarbo-nitrile (HATCN) is a hole-injecting layer, 4,4′,4″-tri(N-carbazolyl)triphenylamine (TCTA) serves as a blocking layer for confining excitons, and NPB and TPBi serve as hole

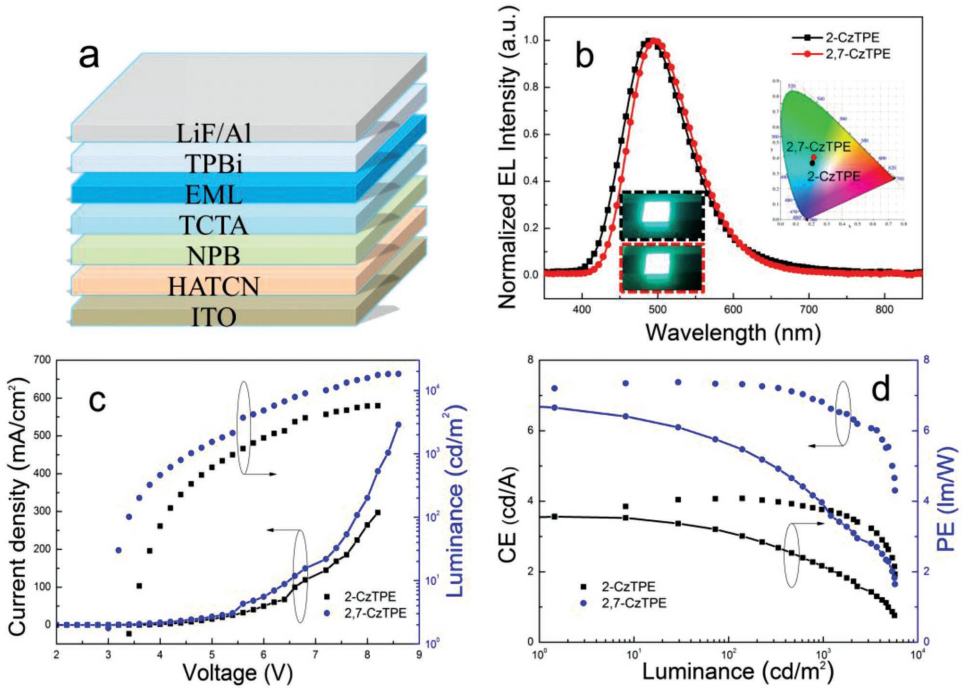

Figure 7. a) The fabricated device structure of the nondoped OLEDs; b) normalized EL spectra for the 2-CzTPE and 2,7-CzTPE-based nondoped OLED devices (the inset shows their corresponding CIE coordinates and explicit photos in devices); c) current density–voltage–luminance (*J*–*V*–*L*) characteristics, and d) current and luminescence efficiency curves for the 2-CzTPE and 2,7-CzTPE-based nondoped OLED devices.

Table 2. Performance of the nondoped OLEDs based on DPVTCz, 2TPE (2,7), 2-CzTPE, and 2,7-CzTPE under the optimized condition.

EMLs	V_{on} [V]	CE_{max} [cd A^{-1}]	PE [lm W^{-1}]	CIE coordinates	EQE [%]	Ref.
DPVTCz	3.8	3.1	–	0.14, 0.22	1.9	[17a]
2TPE (2,7)	4.2	5.5	3.1	0.20, 0.38	–	[17b]
2-CzTPE	3.3	4.08	3.36	0.21, 0.35	1.9	This work
2,7-CzTPE	2.9	7.38	6.81	0.21, 0.40	3.0	This work

and electron-transporting layers, respectively.[28] Although 2,7-CzTPE exhibited the large molecular skeleton compared with 2-CzTPE, the sky-blue emission obtained from both the 2-CzTPE-based and 2,7-CzTPE-based nondoped devices were nearly identical (Figure 7b), which is also similar to the PL spectra, finally leading to the identical CIE coordinates in OLEDs (**Table 2**). Curves of current density–voltage–luminance (*J–V–L*) for the 2-CzTPE-based and 2,7-CzTPE-based nondoped OLED devices were then plotted (Figure 7c) and the corresponding data are tabulated in Table 2. To fully estimate their performance in OLEDs devices, the key performance data for the previously reported DPVTCz and 2TPE (2,7) are also summarized in Table 2.[17] As observed, OLEDs using DPVTCz and 2TPE (2,7) exhibited high turn-on voltages (V_{on}) of 3.8 and 4.2 V, whereas, 2-CzTPE-based and 2,7-CzTPE-based devices in the present study displayed much lower V_{on}, especially for the 2,7-CzTPE-based device (2.9 V), indicating the higher charge injection and much more balanced charge carrier transport caused by its enlarged molecular conjugation. Moreover, the EL performance of 2-CzTPE-based device (CE = 4.08 cd A^{-1}, PE = 3.36 lm W^{-1}, and EQE = 1.9%) was observed to be similar to those of the DPVTCz-based and 2TPE (2,7)-based nondoped OLEDs.[17] By contrast, much better EL performance was achieved for the 2,7-CzTPE-based device with significantly enhanced CE, PE, and EQE values of 7.38 cd A^{-1}, 6.81 lm W^{-1}, and 3.0%, respectively. The results here further demonstrate that 2,7-CzTPE with balanced trade-off between molecular conjugation and twisted conformation not only exhibited highly emissive features in aggregated solid states, but also can significantly enhance the EL performance in its corresponding nondoped OLEDs.

Furthermore, performance in 2,7-CzTPE-based OLEDs with different brightness (100 and 1000 cd m^{-2}) was then compared and their key parameters in device are summarized (Table S1, Supporting Information). Encouragingly, impressive performance with a CE value of 7.21 cd A^{-1}, a PE value of 4.92 lm W^{-1}, and an EQE value of 2.9% can also be obtained at 1000 cd m^{-2} in OLEDs. On the other hand, when the current density was increased from 0.1 to 100 mA m^{-2} in 2-CzTPE-based and 2,7-CzTPE-based nondoped devices, stable EL emissions (especially for 2,7-CzTPE) with nearly identical emission spectra and CIE coordinates were also observed (**Figure 8**). The stable EL performance here in OLEDs for 2,7-CzTPE further suggested its potential as an emitter in the long-lived and high-efficiency nondoped OLEDs devices.

3. Conclusion

In summary, 2-CzTPE and 2,7-CzTPE with promising AIE characteristics were synthesized. Although 2-CzTPE had poor luminescent performance with quantum yield value of 23.12% in solid state and inferior EQE value of 1.9% in OLEDs, 2,7-CzTPE with much balanced molecular conjugation and twisted molecular conformation exhibited significantly enhanced PLQY value of up to 60.63% and also much better EL performance in nondoped OLEDs with maximum CE, PE, and EQE values of 7.38 cd A^{-1}, 6.81 lm W^{-1}, and 3.0%, respectively. Furthermore, the emission for 2,7-CzTPE in both aggregated solid states and OLEDs still remained in the blue region, which is also similar to that in 2-CzTPE, indicating that significantly enhanced luminescent performance can be achieved in the developed 2,7-CzTPE but also retaining its blue emission.

4. Experimental Section

Materials: All these reagents and chemicals were purchased from the commercial sources, such as Aldrich and Acros, and used without further purification, unless otherwise stated. Bromotriphenylethylene was purchased from TCI. Compounds 9-ethyl-2-(4,4,5,5-tetramethyl-[1,3,2]-dioxaborolan-2-yl)-9H-carbazole and 9-ethyl-2,7-bis-(4,4,5,5-tetramethyl-[1,3,2]dioxaborolan-2-yl)-9H-carbazole were easily synthesized according to the literature.[20]

Characterization and Measurement: ^{1}H NMR and ^{13}C NMR spectra were collected using a Bruker ARX 400 NMR; deuterated chloroform

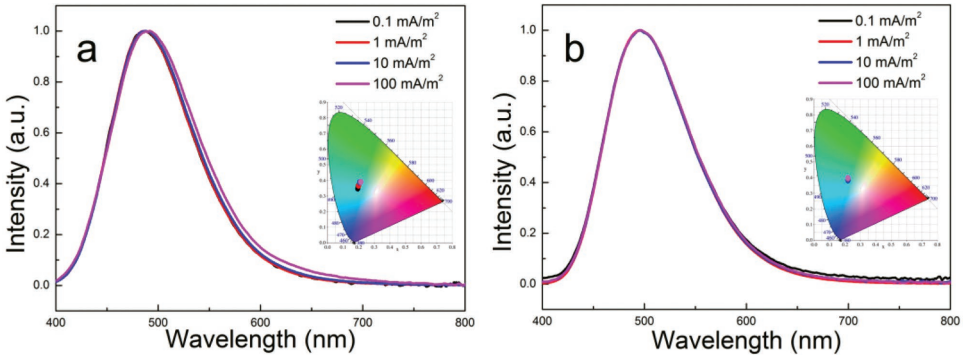

Figure 8. a,b) The EL spectra stability of 2-CzTPE and 2,7-CzTPE-based nondoped OLEDs under different current density (inset is their corresponding CIE coordinates).

($CDCl_3$) was used as a solvent and tetramethylsilane (TMS, $\delta = 0$ ppm) was used as internal standard. High-resolution mass spectra (HRMS) were collected using a GCT premier CAB048 mass spectrometer, operated in MALDI-TOF mode. TGA were performed using a Netzsch TG 209 analyzer. DSC analysis was carried out using a TA Q200 instrument, operated under nitrogen atmosphere and at a heating rate of 10 °C min^{-1}. UV–vis spectra were measured using a Shimadzu UV-2250 spectrophotometer. PL spectra were collected using an Edinburgh Instrument FLS920 fluorescence spectrophotometer. The transient decay spectra were measured using a Fluoro-Cube of HORIBA. The absolute quantum yields in both solution and thin films were obtained by using an Edinburgh Instrument FLS980 Integrating sphere. Fluorescence images were acquired using an Olympus BX 41 fluorescence microscope. SEM images were obtained using a Zeiss GeminiSEM 500. X-ray diffraction patterns were collected using an X-ray diffractometer from New D8 Advance from Bruker. Theoretical study was carried out using the density functional theory (DFT) based on 6-31G** set in Gaussian09, which was approximated by B3LYP. The data collection from single crystals was conducted using a Bruker Smart APEXII CCD diffractometer, equipped with graphite-monochromated Cu Kα radiation (λ = 1.54178 Å). Cyclic voltammograms were performed with a three-electrode electrochemical cell in a 0.1 M tetra(*n*-butyl)ammoniumhexa-fluorophosphate ($TBAPF_6$) solution at a scan rate of 100 mV s^{-1} at room temperature under argon atmosphere. Platinum (Pt) disk, platinum wire, and Ag/AgCl (0.1 M) were used as working electrode, counter electrode, and reference electrode, respectively.

Fabrication of Nondoped OLEDs: The materials were evaporated in a vacuum at 5×10^{-4} Pa (or below) on indium tin oxide (ITO)-coated glass substrates at a sheet resistance of 20 Ω $square^{-1}$. The organic layers were deposited at a rate of 1.0–2.0 Å s^{-1}. The cathode was deposited with LiF (1 nm) at a deposition rate of 0.1 Å s^{-1} and then capped with Al metal (100 nm) using thermal evaporation at a rate of 4.0 Å s^{-1}. The layer thickness of the deposited organic layers was monitored in situ using an oscillating quartz thickness monitor. The EL spectra were measured using a PR705 spectra scan spectrometer. The luminance and current density versus driving-voltage characteristics were recorded by using a Keithley model 2420 source meter. All measurements were carried out at room temperature and under ambient condition.

Synthesis of Compound 2-CzTPE: Under nitrogen atmosphere, to a solution of 9-ethyl-2-(4,4,5,5-tetramethyl-[1,3,2]dioxaborolan-2-yl)-9H-carbazole (1.51 g, 4.67 mmol) and bromotriphenylethylene (1.56 g, 4.67 mmol) in toluene (80 mL) and ethanol (15 mL) was added tetrakis(triphenylphosphine)palladium [$Pd(PPh_3)_4$] (160 mg, 3%) and potassium carbonate (K_2CO_3) (2 M, 23 mL). After stirring at 80 °C overnight, the mixture was cooled down to room temperature (RT) and quenched with water (100 mL). After that, the mixture was extracted with dichloromethane (DCM) three times (3 × 70 mL). Then the resulted organic layer was washed with water (3 × 80 mL) and dried over anhydrous magnesium sulfate ($MgSO_4$). After removing the $MgSO_4$ and solvent, the crude product was obtained and purified using the column chromatography (PE: DCM, *V*:*V* = 6:1) with a yield of 80%. ^{1}H NMR (400 MHz, $CDCl_3$) δ 8.03 (d, J = 7.8 Hz, 1H), 7.87 (d, J = 8.1 Hz, 1H), 7.43 (t, J = 7.2 Hz, 1H), 7.34 (d, J = 8.2 Hz, 1H), 7.20 (t, J = 7.4 Hz, 1H), 7.17–7.01 (m, 16H), 6.92 (d, J = 7.3 Hz, 1H), 4.13 (q, J = 7.2 Hz, 2H), 1.13 (t, J = 7.2 Hz, 3H). ^{13}C NMR (100 MHz, $CDCl_3$) δ 144.25, 144.04, 143.99, 141.94, 141.29, 140.80, 140.37, 139.50, 131.50, 131.44, 131.31, 127.70, 127.66, 127.59, 126.42, 126.35, 126.28, 125.39, 122.76, 122.63, 121.37, 120.30, 119.49, 118.67, 112.08, 108.27, 58.49, 37.25, 18.45, 13.41, 0.95. MS *m*/*z*: M^+ calculated for $C_{34}H_{27}N$, 449.21, found 449.2156.

Synthesis of Compound 2,7-CzTPE: The synthetic route to 2,7-CzTPE is similar to that of 2-CzTPE with a yield of 83%. ^{1}H NMR (400 MHz, $CDCl_3$) δ 7.75 (d, J = 8.1 Hz, 2H), 7.10–7.08 (m, 30H), 7.00 (s, 2H), 6.86 (d, J = 8.1 Hz, 2H), 3.85 (q, J = 7.1 Hz, 2H), 0.84 (t, J = 7.1 Hz, 3H). ^{13}C NMR (100 MHz, $CDCl_3$) δ 144.22, 144.12, 144.02, 141.88, 141.16, 140.68, 139.97, 131.49, 131.43, 131.30, 127.73, 127.64, 127.56, 126.40, 126.32, 126.28, 122.72, 121.19, 119.37, 111.86, 58.51, 36.89, 18.37, 13.10, 1.04, 0.01. MS *m*/*z*: M^+ calculated for $C_{54}H_{41}N$, 703.32, found 703.3229.

Supporting Information

Supporting Information is available from the Wiley Online Library or from the author.

Acknowledgements

This work was supported by the National Basic Research Program of China (973 Program; Grant Nos. 2013CB834701 and 2013CB834702), the University Grants Committee of Hong Kong (Grant No. AoE/P-03/08), the Research Grants Council of Hong Kong (Grant Nos. 16301614, 16305015, and N_HKUST604/14), Innovation and Technology Commission (Grant No. ITC-CNERC14SC01), the National Science Foundation of China (Grant Nos. 81372274, 81501591, 8141101080, and 51603165), the Science and Technology Planning Project of Guangdong Province (Grant Nos. 2014A030313033 and 2014A050503037), and the Shenzhen Science and Technology Program (Grant Nos. JCYJ20130402103240486 and JCYJ20160509170535223). B.Z.T. is also grateful for the support from the Guangdong Innovative Research Team Program of China (Grant No. 201101C0105067115). D.D. also thanks the help from Yanzi Xu and Ruohan Xu in Xi'an Jiaotong University in preparing the samples for PL and SEM measurements.

Conflict of Interest

The authors declare no conflict of interest.

Keywords

aggregation-induced emission, blue emission, luminescent performance, organic light-emitting diodes, organic luminescent materials

Received: June 1, 2018
Revised: June 27, 2018
Published online: August 7, 2018

[1] a) C. W. Tang, S. A. VanSlyke, *Appl. Phys. Lett.* **1987**, *51*, 913; b) S. A. Van Slyke, C. H. Chen, C. W. Tang, *Appl. Phys. Lett.* **1996**, *69*, 2160; c) H. Nakanotani, T. Higuchi, T. Furukawa, K. Masui, K. Morimoto, M. Numata, H. Tanaka, Y. Sagara, T. Yasuda, C. Adachi, *Nat. Commun.* **2014**, *5*, 4016.

[2] a) T. Jüstel, H. Nikol, C. Ronda, *Angew. Chem., Int. Ed.* **1998**, *37*, 3084; b) T. Yu, L. Liu, Z. Xie, Y. Ma, *Sci. China Chem.* **2015**, *58*, 907; c) J. Zhang, B. Xu, J. Chen, S. Ma, Y. Dong, L. Wang, B. Li, L. Ye, W. Tian, *Adv. Mater.* **2014**, *26*, 739; d) Z. Yang, Z. Mao, Z. Xie, Y. Zhang, S. Liu, J. Zhao, J. Xu, Z. Chi, M. P. Aldred, *Chem. Soc. Rev.* **2017**, *46*, 915; e) W. Chen, Y. Yuan, Z. Zhu, Z. Jiang, S. Su, L. Liao, C. Lee, *Chem. Sci.* **2018**, *9*, 4062.

[3] a) K. T. Ly, R. C. Cheng, H. Lin, Y. Shiau, S. Liu, P. Chou, C. Tsao, Y. Huang, Y. Chi, *Nat. Photonics* **2017**, *11*, 63; b) W. Zeng, H. Lai, W. Lee, M. Jiao, Y. Shiu, C. Zhong, S. Gong, T. Zhou, G. Xie, M. Sarma, K. Wong, C. Wu, C. Yang, *Adv. Mater.* **2018**, *30*, 1704961; c) J. Xue, C. Li, L. Xin, L. Duan, J. Qiao, *Chem. Sci.* **2016**, *7*, 2888; d) J. Guo, X. Li, H. Nie, W. Luo, S. Gan, S. Hu, R. Hu, A. Qin, Z. Zhao, S. Su, B. Z. Tang, *Adv. Funct. Mater.* **2017**, *27*, 1606458;

e) J. Guo, X. Li, H. Nie, W. Luo, R. Hu, A. Qin, Z. Zhao, S. Su, B. Z. Tang, *Chem. Mater.* **2017**, *29*, 3623.

[4] a) G. Zhou, W. Wong, B. Yao, Z. Xie, L. Wang, *Angew. Chem.* **2007**, *119*, 1167; b) S. Chen, X. Xu, Y. Liu, G. Yu, X. Sun, W. Qiu, Y. Ma, D. Zhu, *Adv. Funct. Mater.* **2005**, *15*, 1541.

[5] a) Y. Seino, S. Inomata, H. Sasabe, Y. Pu, J. Kido, *Adv. Mater.* **2016**, *28*, 2638; b) K. Guo, H. Wang, Z. Wang, C. Si, C. Peng, G. Chen, J. Zhang, G. Wang, B. Wei, *Chem. Sci.* **2017**, *8*, 1259; c) Y. J. Cho, K. S. Yook, J. Y. Lee, *Adv. Mater.* **2014**, *26*, 4050.

[6] a) Y. Im, S. Y. Byun, J. H. Kim, D. R. Lee, C. S. Oh, K. S. Yook, J. Y. Lee, *Adv. Funct. Mater.* **2017**, *27*, 1603007; b) I. S. Park, H. Komiyama, T. Yasuda, *Chem. Sci.* **2017**, *8*, 953; c) W. Chen, Y. Yuan, S. Ni, Q. Tong, F. Wong, C. Lee, *Chem. Sci.* **2017**, *8*, 3599; d) T. Fleetham, G. Li, L. Wen, J. Li, *Adv. Mater.* **2014**, *26*, 7116; e) X. Tang, Q. Bai, Q. Peng, Y. Gao, J. Li, Y. Liu, L. Yao, P. Lu, B. Yang, Y. Ma, *Chem. Mater.* **2015**, *27*, 7050; f) S. Zhang, L. Yao, Q. Peng, W. Li, Y. Pan, R. Xiao, Y. Gao, C. Gu, Z. Wang, P. Lu, F. Li, S. Su, B. Yang, Y. Ma, *Adv. Funct. Mater.* **2015**, *25*, 1755; g) C. Li, Z. Li, X. Yan, Y. Zhang, Z. Zhang, Y. Wang, *J. Mater. Chem. C* **2017**, *5*, 1973; h) M. Liu, X. Li, D. C. Chen, Z. Xie, X. Cai, G. Xie, K. Liu, J. Tang, S. Su, Y. Cao, *Adv. Funct. Mater.* **2015**, *25*, 5190.

[7] a) B. Liu, H. Nie, X. Zhou, S. Hu, D. Luo, D. Gao, J. Zou, M. Xu, L. Wang, Z. Zhao, A. Qin, J. Peng, H. Ning, Y. Cao, B. Z. Tang, *Adv. Funct. Mater.* **2016**, *26*, 776; b) L. Chen, G. Lin, H. Peng, H. Nie, Z. Zhuang, P. Shen, S. Ding, D. Huang, R. Hu, S. Chen, F. Huang, A. Qin, Z. Zhao, B. Z. Tang, *J. Mater. Chem. C* **2016**, *4*, 5241; c) J. Jiang, D. Hu, M. Hanif, X. Li, S. Su, Z. Xie, L. Liu, S. Zhang, B. Yang, Y. Ma, *Adv. Opt. Mater.* **2016**, *4*, 2109; d) R. Furue, T. Nishimoto, I. S. Park, J. Lee, T. Yasuda, *Angew. Chem., Int. Ed.* **2016**, *55*, 7171.

[8] K. Liu, Z. Xu, M. Yin, *Prog. Polym. Sci.* **2015**, *46*, 25.

[9] a) S. Xue, X. Qiu, Q. Sun, W. Yang, *J. Mater. Chem. C* **2016**, *4*, 1568; b) D. Dang, X. Wang, D. Wang, Z. Yang, D. Hao, Y. Xu, S. Zhang, L. Meng, *ACS Appl. Nano Mater.* **2018**, *1*, 2324; c) L. Sun, T. Liu, H. Li, L. Yang, L. Meng, Q. Lu, J. Long, *ACS Appl. Mater. Interfaces* **2015**, *7*, 4990.

[10] J. Luo, Z. Xie, J. W. Y. Lam, L. Cheng, H. Chen, C. Qiu, H. S. Kwok, X. Zhan, Y. Liu, D. Zhu, B. Z. Tang, *Chem. Commun.* **2001**, *0*, 1740.

[11] a) J. Mei, N. L. C. Leung, R. T. K. Kwok, J. W. Y. Lam, B. Z. Tang, *Chem. Rev.* **2015**, *115*, 11718; b) Y. Hong, J. W. Y. Lam, B. Z. Tang, *Chem. Soc. Rev.* **2011**, *40*, 5361.

[12] a) Z. Zhao, S. Gao, X. Zheng, P. Zhang, W. Wu, R. T. K. Kwok, Y. Xiong, N. L. C. Leung, Y. Chen, X. Gao, J. W. Y. Lam, B. Z. Tang, *Adv. Funct. Mater.* **2018**, *28*, 1705609; b) F. Song, Z. Xu, Q. Zhang, Z. Zhao, H. Zhang, W. Zhao, Z. Qiu, C. Qi, H. Zhang, H. H. Y. Sung, I. D. Williams, J. W. Y. Lam, Z. Zhao, A. Qin, D. Ma, B. Z. Tang, *Adv. Funct. Mater.* **2018**, *28*, 1800051; c) J. Yang, J. Huang, Q. Li, Z. Li, *J. Mater. Chem. C* **2016**, *4*, 2663; d) L. Chen, Y. Jiang, H. Nie, P. Lu, H. H. Y. Sung, I. D. Williams, H. S. Kwok, F. Huang, A. Qin, Z. Zhao, B. Z. Tang, *Adv. Funct. Mater.* **2014**, *24*, 3621; e) Z. Zhao, H. Nie, C. Ge, Y. Cai, Y. Xiong, J. Qi, W. Wu, R. T. K. Kwok, X. Gao, A. Qin, J. W. Y. Lam, B. Z. Tang, *Adv. Sci.* **2017**, *4*, 1700005; f) Q. Li, Z. Li, *Adv. Sci.* **2017**, *4*, 1600484.

[13] X. Tang, L. Yao, H. Liu, F. Shen, S. Zhang, H. Zhang, P. Lu, Y. Ma, *Chem. Eur. J.* **2014**, *20*, 7589.

[14] a) J. Yang, L. Li, Y. Yu, Z. Ren, Q. Peng, S. Ye, Q. Li, Z. Li, *Mater. Chem. Front.* **2017**, *1*, 91; b) B. Liu, H. Nie, G. Lin, S. Hu, D. Gao, J. Zou, M. Xu, L. Wang, Z. Zhao, H. Ning, J. Peng, Y. Cao, B. Z. Tang, *ACS Appl. Mater. Interfaces* **2017**, *9*, 34162.

[15] a) C. Liu, H. Luo, G. Shi, J. Yang, Z. Chi, Y. Ma, *J. Mater. Chem. C* **2015**, *3*, 3752; b) J. Luo, S. Gong, Y. Gu, T. Chen, Y. Li, C. Zhong, G. Xie, C. Yang, *J. Mater. Chem. C* **2016**, *4*, 2442; c) W. Gong, B. Wang, M. P. Aldred, C. Li, G. Zhang, T. Chen, L. Wang, M. Zhu, *J. Mater. Chem. C* **2014**, *2*, 7001; d) H. Mao, C. Zang, G. Shan, H. Sun, W. Xie, Z. Su, *Inorg. Chem.* **2017**, *56*, 9979; e) Z. Zhao, S. Chen, C. Deng, J. W. Y. Lam, C. Y. K. Chan, P. Lu, Z. Wang, B. Hu, X. Chen, P. Lu, H. S. Kwok, Y. Ma, H. Qiu, B. Z. Tang, *J. Mater. Chem.* **2011**, *21*, 10949.

[16] a) Z. Zhao, J. W. Y. Lam, B. Z. Tang, *J. Mater. Chem.* **2012**, *22*, 23726; b) Y. Dong, J. W. Y. Lam, A. Qin, J. Liu, Z. Li, B. Z. Tang, J. Sun, H. S. Kwok, *Appl. Phys. Lett.* **2007**, *91*, 011111.

[17] a) F. Wu, P. Shih, M. Yuan, A. K. Dixit, C. Shu, Z. Chung, E. W. Diau, *J. Mater. Chem.* **2005**, *15*, 4753; b) D. Lo, C. Chang, G. Krucaite, D. Volyniuk, J. V. Grazulevicius, S. Grigalevicius, *J. Mater. Chem. C* **2017**, *5*, 6054.

[18] a) J. Huang, N. Sun, Y. Dong, R. Tang, P. Lu, P. Cai, Q. Li, D. Ma, J. Qin, Z. Li, *Adv. Funct. Mater.* **2013**, *23*, 2329; b) J. Huang, N. Sun, P. Chen, R. Tang, Q. Li, D. Ma, Z. Li, *Chem. Commun.* **2014**, *50*, 2136; c) J. Huang, R. Tang, T. Zhang, Q. Li, G. Yu, S. Xie, Y. Liu, S. Ye, J. Qin, Z. Li, *Chem. Eur. J.* **2014**, *20*, 5317; d) J. Huang, Y. Jiang, J. Yang, R. Tang, N. Xie, Q. Li, H. S. Kwok, B. Z. Tang, Z. Li, *J. Mater. Chem. C* **2014**, *2*, 2028; e) J. Yang, J. Huang, N. Sun, Q. Peng, Q. Li, D. Ma, Z. Li, *Chem. Eur. J.* **2015**, *21*, 6862; f) X. Zhan, N. Sun, Z. Wu, J. Tu, L. Yuan, X. Tang, Y. Xie, Q. Peng, Y. Dong, Q. Li, D. Ma, Z. Li, *Chem. Mater.* **2015**, *27*, 1847.

[19] J. Huang, N. Sun, J. Yang, R. Tang, Q. Li, D. Ma, Z. Li, *Adv. Funct. Mater.* **2014**, *24*, 7645.

[20] a) P. Zhou, D. Dang, Q. Wang, X. Duan, M. Xiao, Q. Tao, H. Tan, R. Yang, W. Zhu, *J. Mater. Chem. A* **2015**, *3*, 13568; b) P. Zhou, D. Dang, M. Xiao, Q. Wang, J. Zhong, H. Tan, Y. Pei, R. Yang, W. Zhu, *J. Mater. Chem. A* **2015**, *3*, 10883.

[21] Z. Zhao, C. Y. K. Chan, S. Chen, C. Deng, J. W. Y. Lam, C. K. W. Jim, Y. Hong, P. Lu, Z. Chang, X. Chen, P. Lu, H. S. Kwok, H. Qiu, B. Z. Tang, *J. Mater. Chem.* **2012**, *22*, 4527.

[22] Y. Yang, X. Su, C. N. Carroll, I. Aprahamian, *Chem. Sci.* **2012**, *3*, 610.

[23] N. L. C. Leung, N. Xie, W. Yuan, Y. Liu, Q. Wu, Q. Peng, Q. Miao, J. W. Y. Lam, B. Z. Tang, *Chem. Eur. J.* **2014**, *20*, 1.

[24] a) W. Liu, Y. Wang, M. Sun, D. Zhang, M. Zheng, W. Yang, *Chem. Commun.* **2013**, *49*, 6042; b) D. Dang, P. Zhou, Y. Wu, Y. Xu, Y. Zhi, W. Zhu, *Phys. Chem. Chem. Phys.* **2018**, *20*, 13171.

[25] D. Dang, Z. Qiu, T. Han, Y. Liu, M. Chen, R. T. K. Kwok, J. W. Y. Lam, B. Z. Tang, *Adv. Funct. Mater.* **2018**, *28*, 1707210.

[26] a) D. Dang, P. Zhou, L. Duan, X. Bao, R. Yang, W. Zhu, *J. Mater. Chem. A* **2016**, *4*, 8291; b) D. Dang, X. Wang, Y. Zhi, L. Meng, X. Bao, R. Yang, W. Zhu, *Org. Electron.* **2016**, *32*, 237.

[27] X. Tang, Q. Bai, T. Shan, J. Li, Y. Gao, F. Liu, H. Liu, Q. Peng, B. Yang, F. Li, P. Lu, *Adv. Funct. Mater.* **2018**, *28*, 1705813.

[28] X. Li, M. Liu, Y. Li, X. Cai, D. Chen, K. Liu, Y. Cao, S. Su, *Chem. Commun.* **2016**, *52*, 14454.

